FLUKA study of the actinides induced irradiation damage in Zircaloy-4 cladding during interim dry storage⋆

M. Marchetti[a,*], S. Manenti[b,c], M. Herm[a] and V. Metz[a]

[a]Karlsruhe Institute of Technology, Institute for Nuclear Waste Disposal, P.O. Box 3640, 76021, Karlsruhe, Germany
[b]Department of Physics, University of Milan, Via Celoria 16, I-20133 Milano, Italy
[c]Laboratorio Acceleratori e Superconduttività Applicata (LASA), Department of Physics, University of Milan and INFN-Milan, Via F.lli Cervi 201, I-20090, Segrate, Italy

ARTICLE INFO

Keywords:
Non-ionising energy loss
Displacements per atom
FLUKA
Dry interim storage
Spent nuclear fuel
Zircaloy-4
Zirconia layer

Abstract

Among the factors influencing the degradation of the spent nuclear fuel cladding in interim dry storage, the irradiation history and the average burnup at discharge must be considered. In fact, due to the pellet-cladding contact particularly affecting high burnup fuels, the inner surface of the cladding becomes increasingly exposed to the damage caused by the alpha decaying actinides present at the rim of the pellet. Moreover, due to the low temperature conditions characteristic of the interim dry storage, thermal recombination of the produced defects is not expected to occur. Here, we investigate the irradiation damage accumulated inside an irradiated Zircaloy-4 cladding 32, 55 and 100 years after the end of irradiation and discharge from the reactor core. The considered cladded UO_2 pellet belongs to a Pressurised Water Reactor (PWR) fuel rod consisting of five segments and having an average burnup at discharge of 50.4 $GWdt_{HM}^{-1}$. The calculations performed with Fluka 2021.2.0 Monte Carlo code show that the volume mostly affected by the irradiation damage corresponds to the ZrO_2 layer formed between the pellet and the cladding. The actinides which are responsible for the alpha damage are mainly ^{242}Cm, ^{244}Cm, ^{241}Pu and ^{238}Pu. The recoiling daughter nuclei during the alpha decays produce irradiation damage only within the first μm of oxide layer.

1. Introduction

After several years of service in a Light Water Reactor (LWR) and successive cooling in a water pool, spent nuclear fuel (SNF) assemblies are loaded into shielded storages casks or dual purpose casks for interim dry storage in several countries such as Belgium, Czech Republic, Germany, Lithuania, South Africa, Spain, Switzerland, Ukraine or United States of America [1–13] . During storage, the SNF experiences auto-irradiation and helium accumulation [14, 15] caused by the alpha decays of the actinides present, in particular, at the periphery of the pellet.

This phenomenon is relevant for high burnup UO_x fuel, which contain high concentration of α-emitting actinides in the rim of the pellet. Moreover, high burnup fuels are characterised by larger volumes due to the swelling caused by the porosity increase, together with the precipitation of insoluble solid fission products and noble fission gases. This in-reactor matrix volume expansion is about 0.8%- 1% per 10 $GWdt_{HM}^{-1}$ [16–18]. The nuclear fuel swelling causes the pellet to enter in contact with the cladding originating pellet-cladding chemical and mechanical interactions (PCI): the fuel becomes progressively bonded to the cladding while oxygen migrates from the pellet to the Zircaloy and an oxide layer progressively forms. Different studies have documented the nature of this oxide layer, finding mainly the existence of ZrO_2 in monoclinic, tetragonal and/or cubic phases [19–25]; strong pellet-cladding bonding through the oxide layer is observed in high burnup fuels [20–22, 25].

After the end of irradiation (EOI) in nuclear reactor, the volume of the fuel is subjected to further increase as a consequence of the accumulation of helium in the fuel matrix plus the expansion of the lattice parameter induced by the alpha damage [14, 15, 26–29]. For high burnup fuels, this additional swelling is prone to worsen the stress borne by the cladding [14] and exposes its inner surface to irradiation damage and defects accumulation.

As the high burnup SNF temperature in interim dry storage slowly decreases from a peak value (at maximum $\sim$ 670 K) to about 450 K and 400 K in, respectively, 40 and 100 years [30–32], thermal annealing of the auto-irradiation induced defects is not expected. In contrast, significant recovery of in-reactor produced defects can be enabled by the

*Corresponding author
mara.marchetti@kit.edu (M. Marchetti); simone.manenti@unimi.it (S. Manenti); michel.herm@kit.edu (M. Herm); volker.metz@kit.edu (V. Metz)

peak temperature [33].
To the authors' knowledge, only a few studies are devoted to the pellet-cladding interface and the impact of the irradiation damage in this area.
Gibert in [34] reports the presence of tetragonal ZrO_2 in the inner surface of the cladding, for a sample extracted from a PWR fuel rod with average burnup of 20 $GWdt_{HM}^{-1}$. Nogita and colleagues [21] observe a cubic zirconia layer for two low burnup fuels; they attribute the lack of monoclinic zirconia (the stable phase for the considered pressure and temperature conditions) to the stabilisation of the cubic phase by fission damage.
Ciszak et al. in [23] perform micro-Raman investigations of the interaction layer existing between a PWR UO_2 fuel and a low tin Zircaloy-4 cladding (average burnup 58.7 $GWdt_{HM}^{-1}$). Here, we identify a zirconia layer of about 15 μm subdivisible in four regions moving from the fuel to the Zircaloy-4: the zone of the cubic zirconia (close to the fuel), tetragonal, monoclinic and a tetragonal phase with signs of irradiation damage. The cubic/tetragonal phases are considered to be stabilized by the fission recoils from the fuel, however, they suggest also irradiation damage as playing a role in the stabilisation process.
In [23] the age of the sample is not reported, however, partial recovery of the defects after removal from the water pool and subsequent auto-irradiation damage cannot be completely excluded.
The determination of the irradiation damage produced at the pellet-cladding interface and the interplay among different physical-chemical parameters (e.g., zirconia phases, hydrides content and their morphology in the cladding) are of paramount importance to predict the cladding physical-mechanical properties and SNF structural integrity during dry interim storage and beyond.
The degradation of the above-mentioned properties can induce the cladding to fail, which represents a matter of concern by considering its role of first barrier against the release of radionuclides. The integrity of the SNF must be ensured during discharging from the nuclear reactor, when transported and placed in interim dry storage, in case of extended interim dry storage [35, 36] and finally during the transfer from interim dry storage to final disposal in a geological repository.
The present article focuses on the irradiation damage produced in a Zircaloy-4 cladding by the actinides decays during the time elapsed after the EOI. A forecast of the irradiation damage accumulated at years 55 and 100 after the end of irradiation is equally provided. For the calculation, the FLUKA Monte Carlo code is used.

2. Material

The present work considers a UO_2 cladded pellet belonging to a fuel rod constituted of five segments and irradiated in the PWR Gösgen (KKG, Switzerland). The fuel, discharged in May 1989 after 1226 effective full power days, is characterised by an average burn-up of 50.4 $GWdt_{HM}^{-1}$ [37]. The pellet under study belongs to a region of the segment displaying a very flat gamma activity profile (see Figure 1), hence an almost constant average burnup [38]. The reported

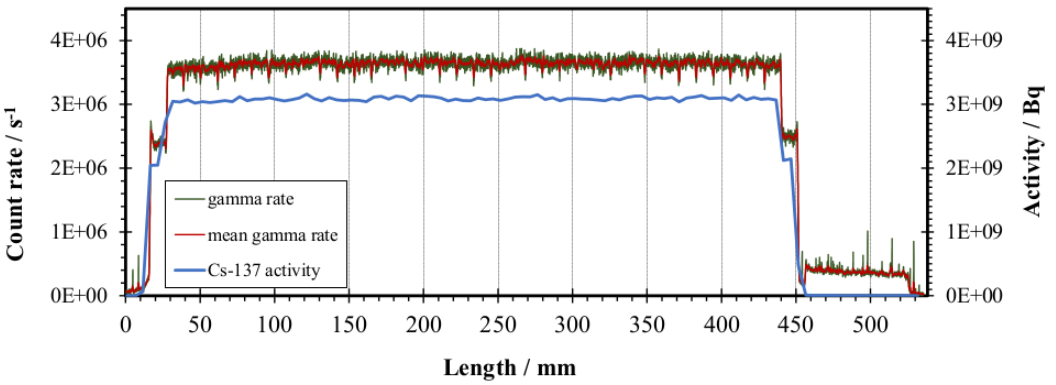

Figure 1: Profile of the γ activity for the considered fuel rod segment. The activity of ^{137}Cs is represented by the blue line; the mean gamma rate is represented by the dark red line on the top. Figure adapted from [38]

initial Zircaloy-4 cladding internal and external diameters are, respectively, 9.28 mm and 10.75 mm. Measurements

performed after 20-30 years from the end of irradiation (in the present measurements campaign and in [38]) display external diameter values within the range 10.66-10.90 mm; for the simulation the initial external diameter of 10.75 mm is chosen. Due to the lack of precise knowledge of the Zircaloy-4 composition for the fuel rod under study, the standard Zircaloy-4 composition in Table 1 is considered, according to [39, 40]. Here, the chosen Sn content is the minimum reported value in [39]. The density of the Zircaloy-4 is considered to be 6550 kg m^{-3} [41].

Table 1
Content of alloying elements (weight %) used in the simulations for the studied Zircaloy-4.

Sn	Fe	Cr	O
1.2 %	0.24 %	0.13 %	0.16 %

Post-irradiation examinations of this specific segment are ongoing; thus, the extent of ZrO_2 at the pellet-cladding interface is still unknown. To estimate the ZrO_2 thickness, the scanning electron microscope image in Figure 2 (c), acquired in the nineties of last century on a sample from a twin segment (Figures 2 (a) and (b)) [42], was analysed by means of Fiji 1.53f51 [43]. According to the analysis, the zirconia layer is approximatively 15 μm thick; this value is perfectly consistent with results reported by Ciszak et al. [23] for a PWR fuel with comparable average burnup.
For the ZrO_2 layer the theoretical density of the cubic structure is chosen (6081 kg m^{-3} [44]), since it is contained between the two limiting values of monoclinic and tetragonal zirconia theoretical densities [45].

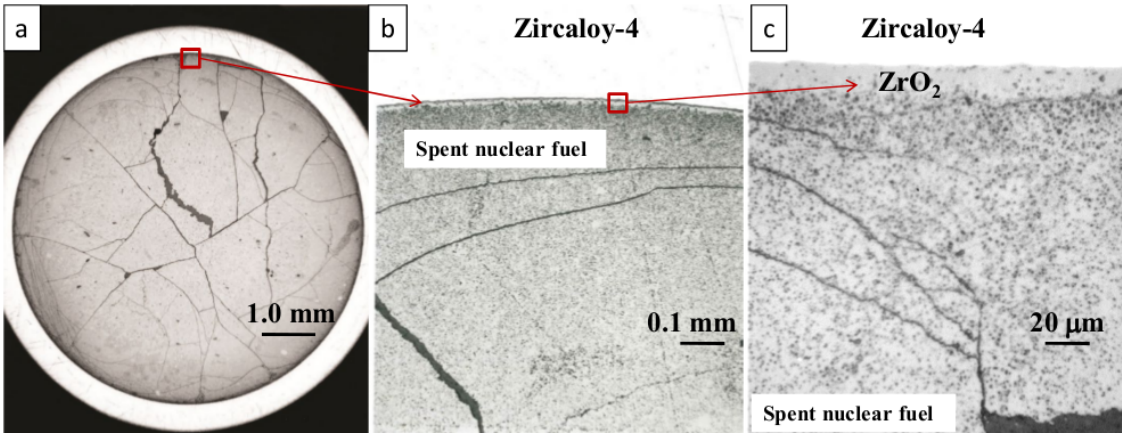

Figure 2: Scanning electron microscope micrographs of a sample extracted from a twin fuel rod segment (adapted from [42]). (a) Cross section (b) and (c) Higher magnification images depicting the interface between the Zircaloy-4 cladding and the uranium dioxide pellet. The images show a layer of about 15 μm of thickness between the pellet and the Zircaloy-4 cladding attributable to the zirconia layer.

3. FLUKA simulations

The FLUKA Monte Carlo code is a particle physics simulation package for particle transport and interaction with matter.
The code is applicable to a wide range of fields and can simulate about 60 different particles, including photons, electrons (from 1 keV to thousands of TeV), and hadrons of energies up to 20 TeV [46, 47]; the emitted radiation from unstable residual nuclei can be tracked online. This code can be coupled with FLAIR graphical user interface [48] which enables the user to define the *input file*, where materials, geometry, particle type/energy and the scoring mesh can be defined, together with the number of primaries and cycles.
FLUKA can use radionuclides as sources and simulates their decays in two manners: *a*) by analytically solving the Bateman equations *b*) by performing a *semi-analogue* simulation; i.e, the code randomly samples the nature of the decay and the corresponding decay times following the modus operandi of Monte Carlo with all unstable nuclei. The particles emitted during the decay are transported together with the other secondaries [49].

Currently, if the radionuclide is chosen as source (beam), the analytical solution option cannot be activated, hence, in the present work, irradiation damage caused by the actinides as sources is obtained by selecting the *semi-analogue* mode; the correct cooling time is set through the option TCQUENCH, which interrupts the scoring at the desired time interval. The code does not transport the daughter nucleus after the radioactive decay, but only the heavy ions produced in the prompt part of the simulation contribute to the damage calculations. Thus, the contribution of the daughter nuclei is herein included by simply selecting a beam of daughter nuclei; the results is then normalised by taking into account the number of alpha decays occurred within the timeframe of interest (the details are offered in section 5).
Transport and in-flight decay of excited residual nuclei are enabled. The simulations are executed for five cycles with 250 000 primaries except for ^{243}Am and ^{242}Pu, which have 500 000 and 1 000 000 primaries, respectively. The calculations are performed with FLUKA 2021.2.0 interfaced with FLAIR 2.3-0 through a Linux Ubuntu operating system.

4. Irradiation damage

Radiation interacting with a crystalline material can produce defects in its lattice which are classifiable in two macro-categories: point defects (e.g, missing/incorrectly positioned atoms) and extended defects (e.g, dislocations, grain boundaries, precipitates or voids) [50]. These defects are a consequence of the energy transferred by the projectile to the target during the physical interaction.
Generally, particles penetrating matter with energy greater than ∼100 eV [51] lose energy either by exciting and ionising atomic electrons or by colliding with the material nuclei and partially inducing displacements of atoms from their original site. These displacements are the main responsible for the damage occurring in the target.
To quantify the second of the above-mentioned processes the non-ionising energy loss concept (NIEL) was introduced [52]. The NIEL depends upon the Lindhard partition function $\xi(T)$ which is in turn defined by the ratio between nuclear and total stopping powers. However, the non-ionising energy losses below the material threshold displacement energy (E_{th}) generate phonons and do not lead to material damage; furthermore, ballistic recombinations of produced defects are a realistic scenario [53, 54].
The measure mostly used to quantify irradiation damage is the displacements per atom (dpa). According to the NRT model [55] the dpa can be calculated as [54]:

$$dpa = \frac{A}{N_A\,\rho}\,0.8\,\frac{\xi(T)\,T}{2E_{th}} \tag{1}$$

where A and ρ define, respectively, the molar mass and the density of the material, N_A the Avogadro number, T the kinetic energy of the primary knock-on-atom (the first atom colliding with the projectile) and E_{th} the displacement damage threshold. The NRT model considers binary collisions where energy transfer cross-sections can be derived from the hard-sphere model and the energy is not deposited in the lattice. The factor 0.8 in equation 1 represents the displacement efficiency and takes into account the possibility of ballistic recombination of defects within the cascade [56].
The dpa calculated according to the NRT model, is based on the *unrestricted* in energy nuclear stopping power and considers also recoils with kinetic energy smaller than the damage threshold. Moreover, the displacement efficiency is in reality dependent on the kinetic energy T, in particular when $T \geq 2$ keV [54]. As a result, the NRT-dpa represents an over-prediction of the produced stable defects: as the primary knock-on atom energy increases, the density of Frenkel defects (vacancies and interstitials) tends to be higher inducing important recombination events once the cascade atom energies are below the displacement damage threshold [57].
For a more realistic physical description, FLUKA implements a correction factor for the displacement efficiency which takes into account the larger recombination probability of defects at higher kinetic energies and uses the *restricted* in energy nuclear stopping power, disregarding the recoils with $T \leq E_{th}$ [54].

5. Displacements per atom calculation

The geometry used in the simulation is schematised in Figure 3 and represents a nuclear fuel pellet having 11.5 mm of height, surrounded first by a zirconia layer 15 μm thick (black lines in 3) and by a second layer representing the Zircaloy-4 cladding (white areas). In the calculation, the penetration of the ZrO_2 in the fuel, as reported in [25], is considered to be 5 μm, while the zirconia penetration in the cladding is 10 μm; hence, the thickness of the Zircaloy-4

metallic wall is accordingly reduced.
The threshold displacement energy is set to 40 eV for Zr, Fe, Cr [58, 59] and 20 eV for O and Sn [15, 59, 60]. Concerning the properties of the UO_2, the density of the rim, due to the high burnup structure [61, 62], is entered in the input file as 0.75 times the UO_2 theoretical density (10960 $\mathrm{kg\,m^{-3}}$). The correction factor is derived by inserting a fractional porosity (p) of 0.21 reported in [63] in the empirical correlation introduced in [18, 64]:

$$\rho = 10960\,(1 - 8 \cdot 10^{-4} burnup)\,(1 - p) \tag{2}$$

where the *burnup* is expressed in $\mathrm{GWdt_{HM}^{-1}}$.
The actinides activity concentrations at the EOI were mainly extracted from the radiochemical analyses of specimens sampled from the rim zone of the twin segment reported in [65]; in particular ^{238}Pu, ^{239}Pu,^{241}Pu, ^{241}Am, ^{242}Cm and ^{244}Cm. The activity concentrations of ^{240}Pu, ^{242}Pu, ^{243}Am, ^{243}Cm, ^{245}Cm and ^{246}Cm were obtained by using Webkorigen [66, 67] in NUCLEONICA [68]. In the latter case the activity concentration is not specific to the periphery of the pellet, hence represents an estimation of the possible actual values.
The activities of the radionuclides were normalised to the mass of heavy metal in the last 50 μm of the pellet rim.
The contribution of the recoiling nuclei to dpa was considered by using the same geometry and a beam of daughter nuclei: here, the dpa was successively normalised to the number of alpha decays occurred in the specific time frame weighted for a 0.5 probability of recoiling in the target direction.

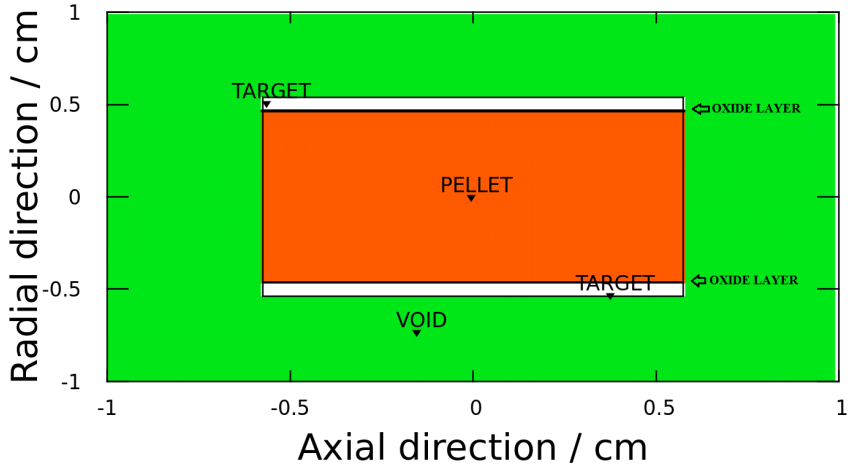

Figure 3: Schematic of geometry used in the present work to simulate the nuclear fuel pellet object of study. The orange central area represents the UO_2 nuclear fuel, the white areas indicate the Zircaloy-4 cladding, while the two black slices between Zircaloy-4 and the UO_2 pellet constitute the ZrO_2 oxide layer. The void (in green) surrounds the cladded pellet.

The number of alpha decays during ∼32, 55 and 100 years was obtained by means of Decay Engine++ of NUCLEONICA [68].
A comparison between the alpha spectra of two sample actinides, i.e., ^{238}Pu and ^{244}Cm, is enabled by Figures 4 and 5.

Here, it emerges that albeit the majority of scored alpha particles are in the energy range 3 - 5.5 MeV in both cases, ^{244}Cm produces a higher number of alphas per primary in the 5.5 - 9 MeV interval. Moreover, the maximum alpha energy for the considered Cm isotope is 8.9 MeV deriving from the ^{212}Po decay, whilst for the ^{238}Pu decay chain is 7.7 MeV from ^{214}Po. In this context, a larger penetration in the target of the irradiation damage is expected from the decay of ^{244}Cm with respect to ^{238}Pu.
Depicted in Figure 6 are the dpa produced at the pellet-cladding interface/inner surface of the cladding, after 32 years of storage, by the alpha-decays of Am, Pu and Cm isotopes, taking into account their inventory at the EOI. In these calculations, the effects of the recoiling daughter nuclei are not included.
The three graphs of Figure 6 highlight the larger irradiation damage (in terms of dpa) produced by the Cm isotopes with respect to Pu and Am isotopes; in particular, the dpa produced by the Pu isotopes are about 650 times larger than those due to Am and 26 times smaller than dpa produced by Cm isotopes, in the first dozens of micrometres. The

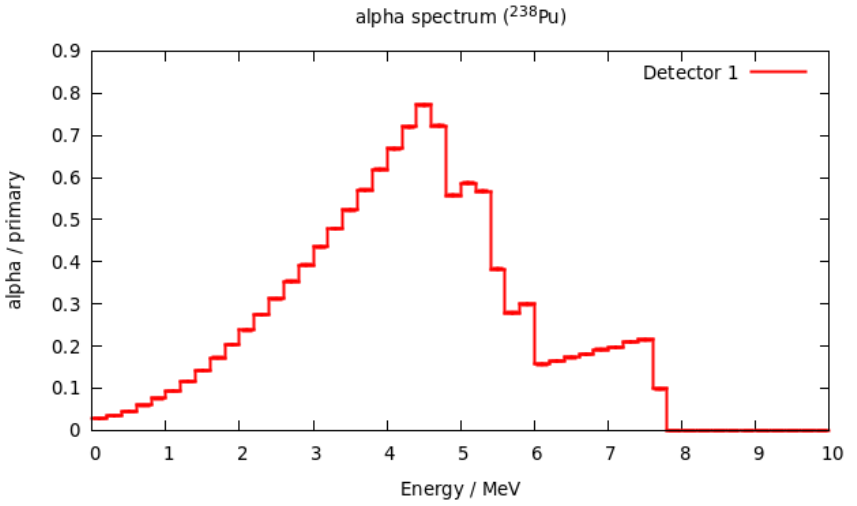

Figure 4: Spectrum of the alphas per primary in the zirconia layer originated by the ^{238}Pu decay. Detector 1 defines the ideal detector collecting the different alpha particles.

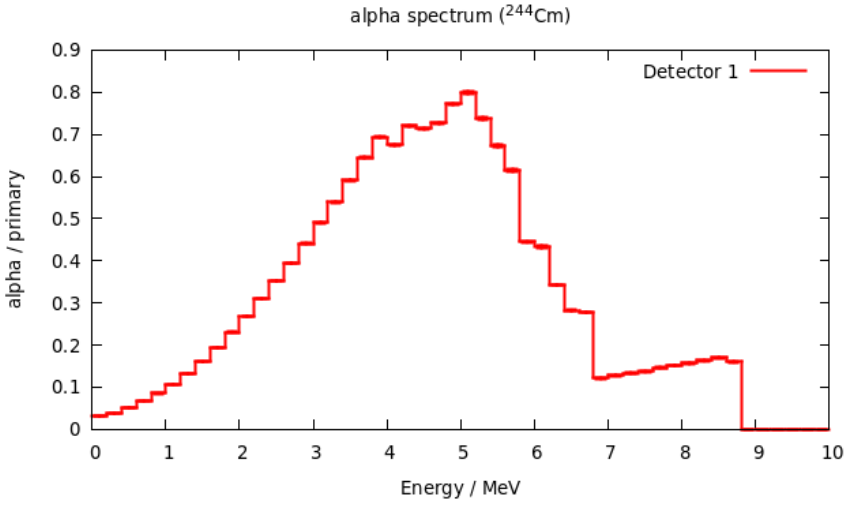

Figure 5: Spectrum of the alphas per primary in the zirconia layer deriving from the ^{244}Cm decay. Detector 1 defines the ideal detector collecting the different alpha particles.

main contribution to damage in 32 years derives from ^{242}Cm and ^{244}Cm. The penetration of the irradiation damage in depth covers mainly the zirconia layer and only in the case of Cm isotopes extends beyond in the Zircaloy-4 material.

The dpa calculated in the frame of the present simulation represent more realistic values in comparison with the dpa inferable from the NRT theory. However, the NRT theory dpa can be obtained by using the deposited, unrestricted, non-ionising energy losses (NIEL-DEP in the code) in equation 1. Figure 7 shows the NIEL-DEP values for the radionuclides producing significant dpa.
^{242}Cm and ^{244}Cm deposit the largest fraction of unrestricted non-ionising loss: they present both the highest NIEL-DEP per primary together with a large concentration in the rim. The large concentration of ^{241}Pu in the rim is responsible for its higher deposition of non-ionising energy losses in comparison with ^{241}Am or ^{238}Pu; as expected by observing the decay chain, ^{241}Am and ^{241}Pu show comparable NIEL-DEP per primary.

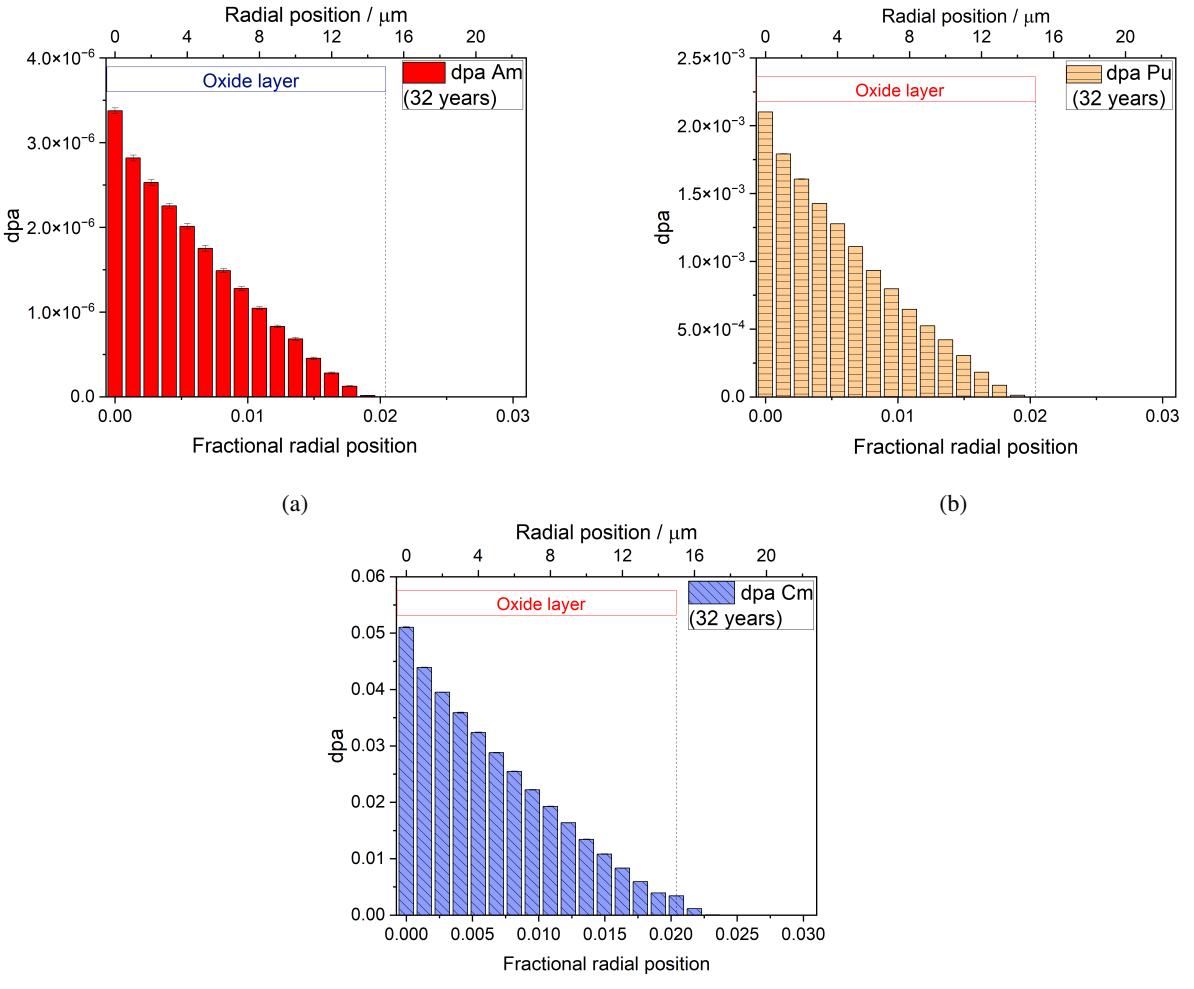

Figure 6: Displacements per atoms (dpa) produced at the pellet-cladding interface/ inner surface of the cladding in 32 years of storage. (a) dpa due to the alpha decays of ^{241}Am and ^{243}Am (b) dpa caused by the alpha decays of the ^{238}Pu, ^{239}Pu, ^{240}Pu, ^{241}Pu and ^{242}Pu. (c) dpa produced by the alpha decays of the ^{24x}Cm, with $2 \leq x \leq 6$). The fractional radial positions are measured from the edge of the UO_2 pellet.

A forecast of the irradiation damage in terms of dpa produced 55 and 100 years after the EOI is presented in Figures 8 and 9.

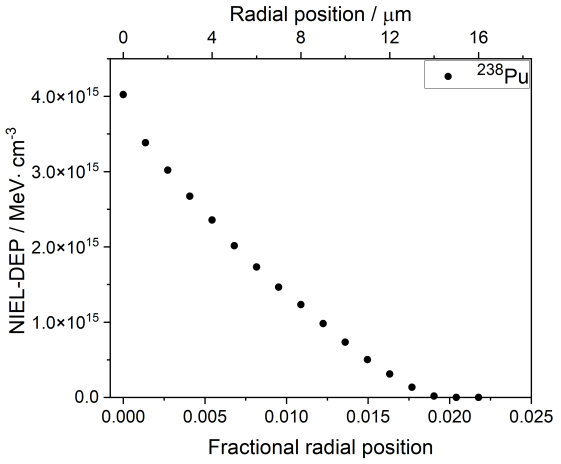

(a)

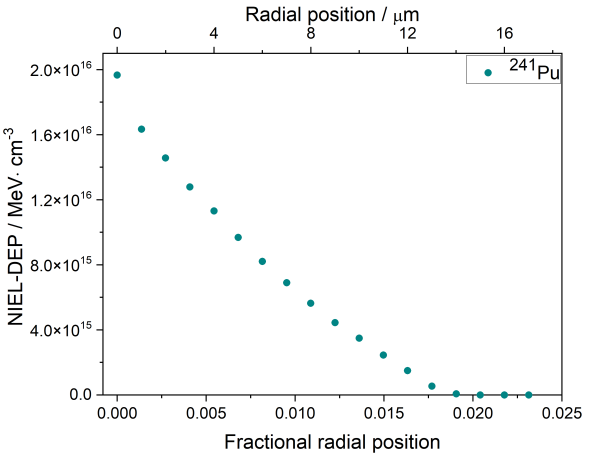

(b)

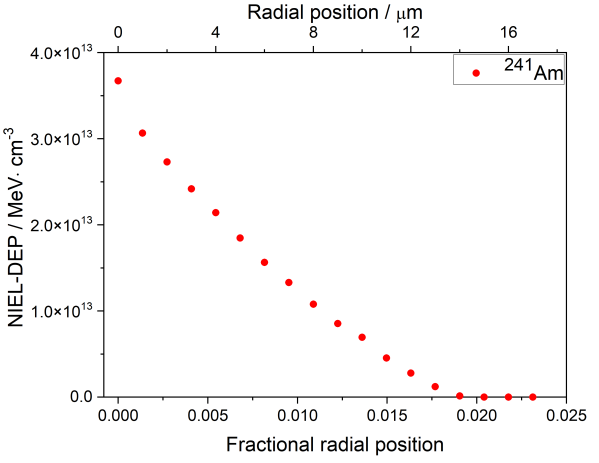

(c)

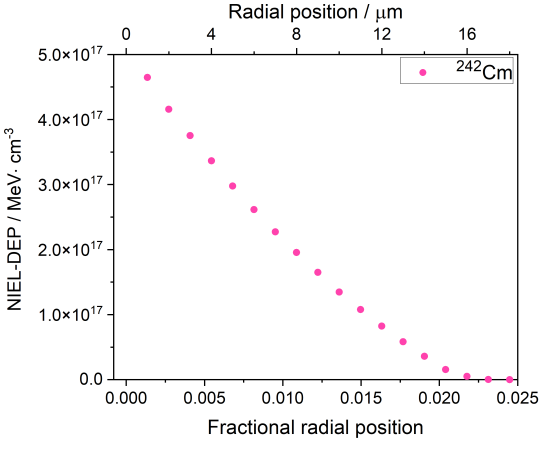

(d)

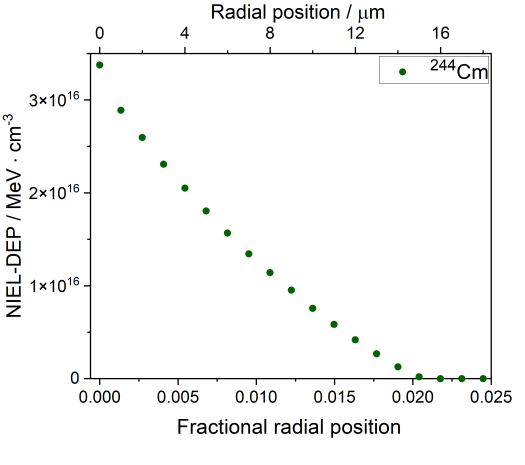

(e)

Figure 7: Unrestricted, non-ionising, energy loss deposited (NIEL-DEP) at the pellet-cladding interface/inner surface of the cladding in 32 years of storage. NIEL-DEP due to decays of: (a) ^{238}Pu, (b) ^{241}Pu, (c)^{241}Am, (d) ^{242}Cm and (e) ^{244}Cm. The fractional radial positions are measured from the edge of the UO_2 pellet.

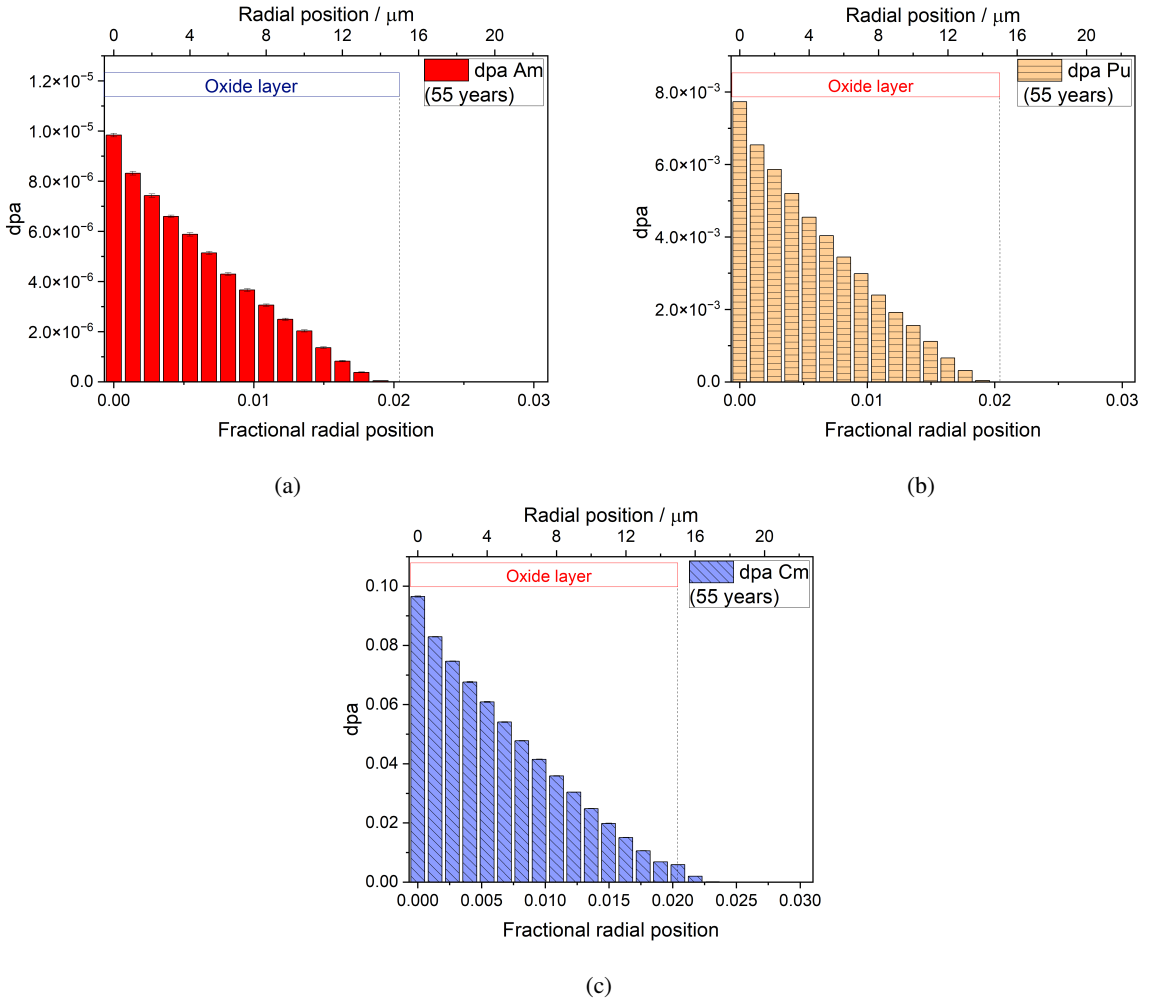

Figure 8: Displacements per atoms (dpa) produced at the pellet-cladding interface/ inner surface of the cladding in 55 years of storage. (a) dpa due to the alpha decays of ^{241}Am and ^{243}Am (b) dpa caused by the alpha decays of the ^{238}Pu, ^{239}Pu, ^{240}Pu, ^{241}Pu and ^{242}Pu. (c) dpa produced by the alpha decays of the ^{24x}Cm, with $2 \leq x \leq 6$). The fractional radial positions are measured from the edge of the UO_2 pellet.

At the second time step, $\frac{\text{dpa (Pu)}}{\text{dpa (Am)}}$ increases to about 800 whilst $\frac{\text{dpa (Cm)}}{\text{dpa (Pu)}}$ drops to about 14. In the year 100, this variation is even more pronounced since $\frac{\text{dpa (Pu)}}{\text{dpa (Am)}} \sim 960$ and $\frac{\text{dpa (Cm)}}{\text{dpa (Pu)}} \sim 8$. The effect is consistent with the ^{241}Am build-up occurring between 32 and 100 years caused by the ^{241}Pu beta decay, while the observed decrease in the ratio between dpa (Cm) and dpa (Pu) is explainable with the decline of the alpha activities of all the Cm isotopes with the exception of ^{245}Cm and ^{246}Cm (see Figure 10).

During the alpha decay, the He nucleus loses its energy mainly by ionisation and excitation processes in the target; only a small fraction of energy losses is available for elastic nuclear collisions and atom displacements. On the contrary, the heavy daughter nucleus has a recoiling energy of $\frac{m_\alpha}{m_D} \cdot T_\alpha \sim 90$ - 100 keV (m stands for mass, D for daughter), which is primarily lost in elastic nuclear interactions. The consequence is a very high number of displacements produced by the recoiling daughter nuclei; nonetheless, this process takes place in a range shorter than 50 nm. Therefore, the dpa caused by the recoiling nuclei are computed only in the first μm of the zirconia layer, namely the first bin for the calculation. Table 2 illustrates the dpa induced by the recoiling daughter nuclei in the first region: dpa increases between 32 and 55 years in a fashion that is almost perfectly mirrored in the interval between 55 and 100 years, namely a dpa rise of $\sim 50\,\%$ occurs between each time step.

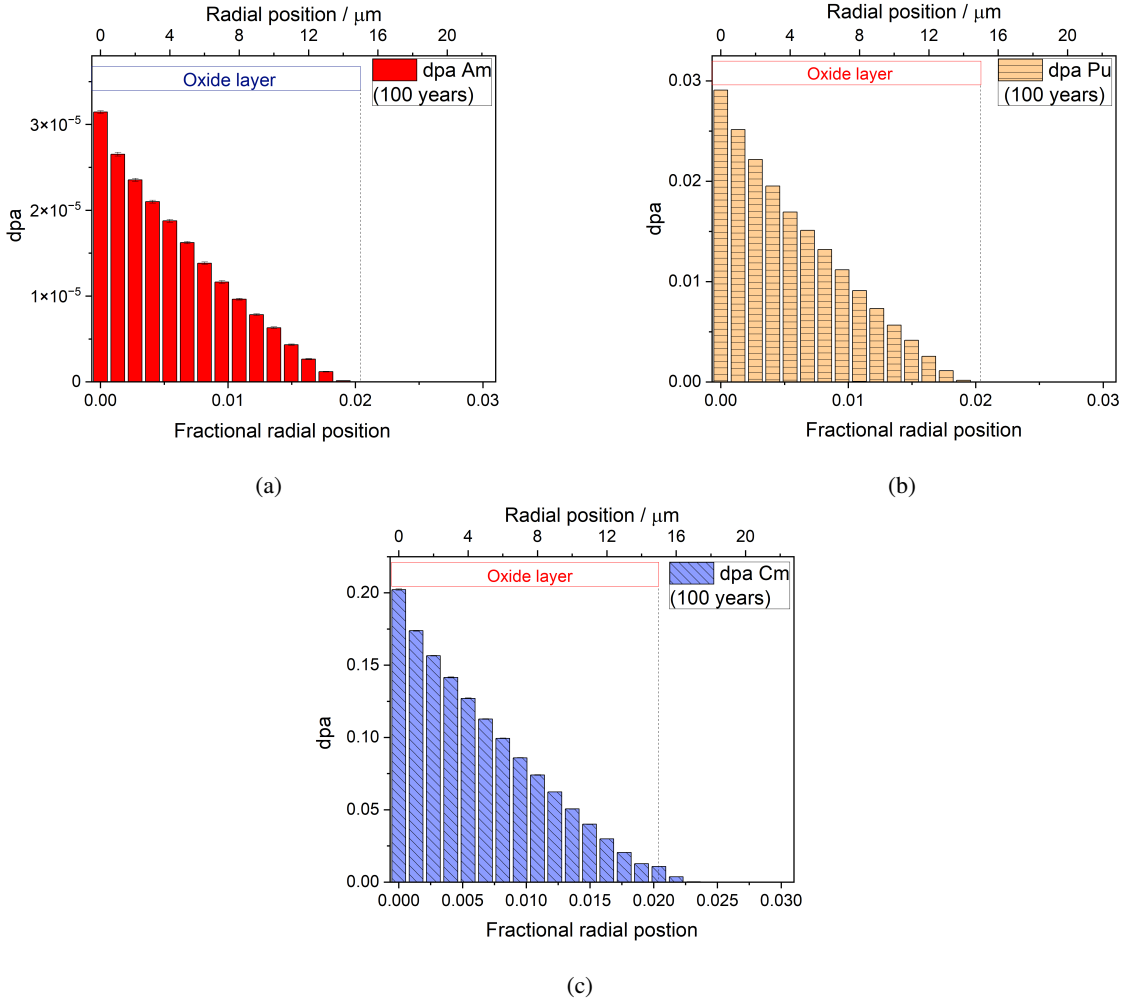

Figure 9: Displacements per atoms (dpa) produced at the pellet-cladding interface/ inner surface of the cladding in 100 years of storage. (a) dpa due to the alpha decays of ^{241}Am and ^{243}Am (b) dpa caused by the alpha decays of the ^{238}Pu, ^{239}Pu, ^{240}Pu, ^{241}Pu and ^{242}Pu. (c) dpa produced by the alpha decays of the ^{24x}Cm, with $2 \leq x \leq 6$).The fractional radial positions are measured from the edge of the UO_2 pellet.

Table 2
Total dpa produced by the recoiling daughter nuclei of Am, Cm and Pu isotopes at 32, 55 and 100 years after the EOI calculated in the first μm from the fuel pellet edge.

32 years	$7.17 \cdot 10^{-3} \pm 0.02 \cdot 10^{-3}$
55 years	$1.08 \cdot 10^{-2} \pm 0.01 \cdot 10^{-2}$
100 years	$1.66 \cdot 10^{-2} \pm 0.01 \cdot 10^{-2}$

The values of Table 2 are added to the dpa generated mainly by the alpha decays in Figure 11, simultaneously for the three considered time intervals. Excluding the first bin of 1 μm, the displacements per atom increase induced by alpha auto-irradiation is about 90 % between 32 and 55 years and 120 % between 55 and 100 years. The first μm is subjected to the additional damage caused by the recoiling daughter nuclei, however, this damage might extend more in depth due to the real interpenetration between the ZrO_2 and the UO_2 at the pellet-cladding interface observed in high burnup fuels [25]. Notwithstanding the fall in the alpha activities of ^{242}Cm and ^{244}Cm, the displacements per atom generated at the level of the Zircaloy-4 are 70 % higher after 55 years in respect of 32 years and 80 % higher after 100

years in comparison with the intermediate time interval: the irradiation damage at the level of Zircaloy-4 continues to accumulate during the time frame of interest for the interim dry storage (particularly for the extended interim dry storage). The irradiation damage produced by non-ionising energy losses and expressed in terms of dpa penetrates the pellet-cladding interface and inner surface of the cladding for less than 2.5 % in depth in each considered time interval. This is reasonable if one considers that alpha particles and heavy ions lose most of the energy in a very short range; however, the number of displacements and irradiation damage produced in this area is significant and might lead to physical-chemical alterations in the considered material.

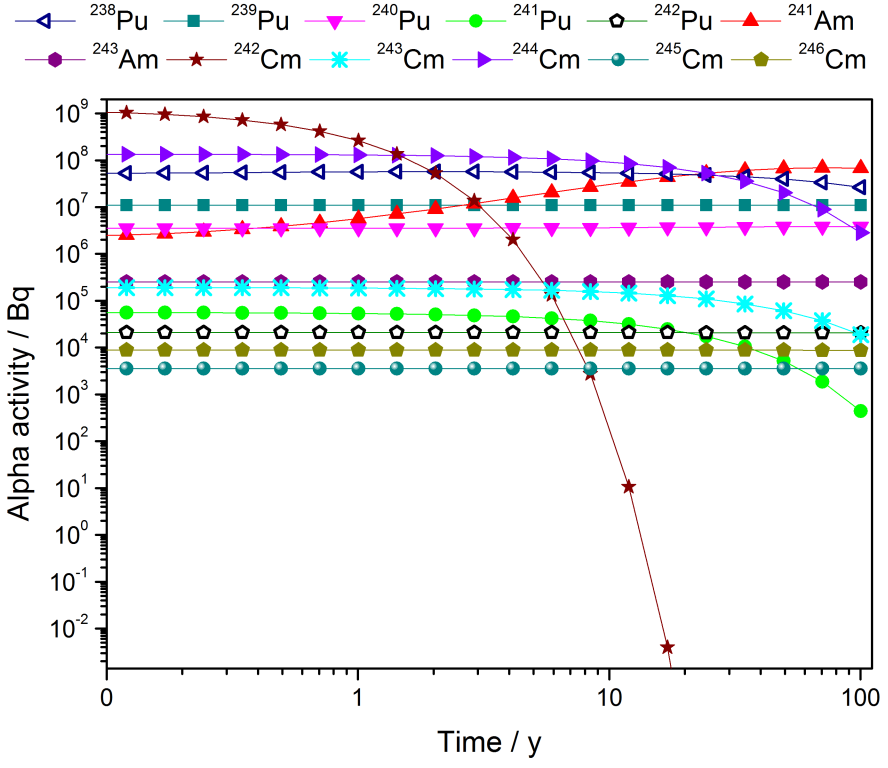

Figure 10: Alpha activity during 100 years calculated by DECAY ENGINE++ for the ^{241}Am, ^{243}Am, ^{238}Pu - ^{242}Pu and ^{24x}Cm with $2 \leq x \leq 6$ inventory in the considered nuclear fuel pellet.

6. Conclusions

In the present work the displacements per atom (dpa) produced at the pellet-cladding interface/inner surface of the cladding, during 32, 55, 100 years of SNF storage, are calculated by means of FLUKA 2021.2.0 Monte Carlo code. First, the code presents the advantage of accurately calculating the dpa by accounting for recombination effects and their dependence on the kinetic energy of the primary knock-on atom. Second, FLUKA correctly disregards the recoiling particles possessing kinetic energy below the threshold damage energy. The displacements per atom generated by alpha, beta particles and heavy ions, produced in the prompt part of the simulation, can be directly scored by the code; nonetheless, the daughter nuclei in the radioactive decay are not transported and the dpa in the target deriving from this component of the radioactive decay is separately estimated.

The simulations pinpoint that in 32 years the largest non-ionising energy losses are deposited by ^{242}Cm and ^{244}Cm, followed by ^{241}Pu, ^{238}Pu, and ^{241}Am. The high concentration of ^{241}Pu in the periphery of the pellet determines its generally significant contribution to the deposited non-ionising energy losses.

The irradiation damage reported in terms of displacements per atoms is mainly produced at the level of zirconia layer at the pellet-cladding interface and penetrates in the Zircaloy-4 material only as a consequence of the Cm isotopes decay, as expected by qualitative comparing the alpha spectra of ^{238}Pu and ^{244}Cm. This penetration does not exceed

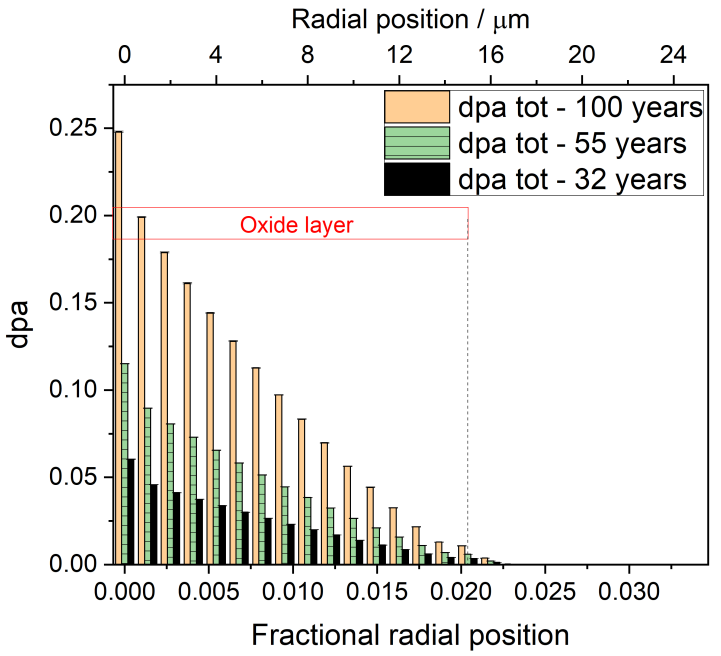

Figure 11: Total dpa calculated by summing the dpa produced by all the radio-isotopes considered in the present simulation.The black bars refer to the year 32, the green bars indicate the year 55 whilst the light pink bars define the year 100. The first bar considers also the dpa produced by the recoiling daughter nuclei.

2.5 % of thickness, starting the measurement from the uranium dioxide pellet border.
Comparisons performed between the three time intervals indicate that the contribution to displacements per atom of ^{242}Cm and ^{244}Cm decreases with time due to their progressive decay, while the contribution of ^{241}Pu rises due to the continuous accumulation of ^{241}Am in the decay chain.
By analysing the accumulated total dpa after 32, 55 and 100 years, one can affirm that in general the damage significantly augment by $\sim 90\,\%$ of the initial value between the first and the second time step and $\sim 120\,\%$ between 55 and 100 years; considering the absolute values, the majority of displacements are occurring in the last 45 years.
The determination of the irradiation damage in terms of dpa is important to understand the evolution of the physical-chemical and, consequently, mechanical properties of the cladding under interim dry storage, particularly focusing on the critical area of the pellet-cladding interface, where physical, chemical and mechanical interactions take place.
As observed by the authors in the open literature [20, 23, 24, 34], the inner ZrO_2 presents structures that are not normally stable under the temperature and pressure conditions of the examinations (i.e., cubic and tetragonal phases). One can assume that recoiling atoms acting as dopants and irradiation damage produced after the EOI could contribute to the preferential stabilisation of one zirconia structure over the other.
Concerning the mechanical properties variation in the inner surface of the cladding, it is important to stress that the type of damage cannot be directly inferred from the dpa level, since the type of damage is also correlated to the local temperature induced by the projectile interaction. In particular, this local temperature might increase when energy is predominantly lost due to electronic stopping. However, the present study considers particles having comparable energies and masses: the above-mentioned possible difference can be attributed to alpha particles versus recoiling daughter nuclei and it is negligible beyond the first μm in depth in the zirconia layer.
Post irradiation examinations of the pellet-cladding interface will single out the physical/mechanical properties variation correlated to the irradiation damage level reached 32 years after the EOI.

7. Acknowledgements

The authors convey their gratefulness to the FLUKA developers, particularly P. R. Sala and A. Ferrari for the elucidations received. D.H. Wegen, D. Papaioannou, R. Nasyrow, R. Gretter, W. de Weerd, S. Bremier and D. Pellottiero are gratefully acknowledged for measuring the γ activity profile and the porosity of the studied fuel rod segment.

CRediT authorship contribution statement

M. Marchetti: Conceptualisation, Methodology, Investigation, Formal Analysis, Validation, Data Curation, Visualisation, Writing-Original, Editing. **S. Manenti:** Methodology, Resources, Visualization, Validation, Writing-Review. **M. Herm:** Resources, Data Curation Writing-Review. **V. Metz:** Resources, Data Curation, Visualization, Writing-Review.

References

[1] S. V. Alyokhina, Problems of creating scientific and methodological bases of spent nuclear fuel dry cask storage thermal safety in Ukraine, Проблеми машинобудування 21 (2018) 4–12.

[2] V. Fajman, L. Bártak, J. Coufal, K. Brzobohatý, S. Kuba, Czech interim spent fuel storage facility: operation experience, inspections and future plans, in: IAEA-TECDOC–1089, IAEA, International symposium on storage of spent fuel from power reactors; Vienna (Austria); 9-13 Nov 1998, 1999, pp. 29–39.

[3] J. A. Gago, J. M. Gravalos, P. Zuloaga, Status on spent fuel management in Spain, in: Storage of spent fuel from power reactors, IAEA-TECDOC–1089, IAEA, International symposium on storage of spent fuel from power reactors; Vienna (Austria); 9-13 Nov 1998, 1999, pp. 125–128.

[4] IAEA, Operation and Maintenance of Spent Fuel Storage and Transportation Casks/Containers, Technical Report, IAEA-TECDOC-1532, 2007.

[5] OECD-NEA, The Safety of Long-Term Interim Storage Facilities in NEA Member Countries, Technical Report, NEA/CSNI/R(2017)4, 2017.

[6] V. Maree, A. Carolissen, The management of used (Spent) Fuel and high level waste in South africa, in: Disposal of High Level Waste Including Spent Nuclear Fuel, IAEA-CN–242, International Conference on the Safety of Radioactive Waste Management; Vienna (Austria); 21-25 Nov, 2016, pp. 64–68.

[7] V. Penkov, R. Diersch, The dry spent RBMK fuel cask storage site at the ignalina NPP in lithuania, in: Storage of spent fuel from power reactors, IAEA-TECDOC–1089, nternational symposium on storage of spent fuel from power reactors; Vienna (Austria); 9-13 Nov 1998, 1999, pp. 103–109.

[8] P. Poskas, Progress on Nuclear Waste Management, Springer Fachmedien Wiesbaden, Wiesbaden, 2018, pp. 139–160. doi:10.1007/978-3-658-21441-8_7.

[9] D. Köhnke, M. Reichardt, F. Semper, Zwischenlagerung Hoch Radioaktiver Abfälle, Springer, 2017. doi:https://doi.org/10.1007/978-3-658-19040-8.

[10] D. B. Rigby, Evaluation of the technical basis for extended dry storage and transportation of used nuclear fuel: executive summary, US Nuclear Waste Technical Review Board, 2010.

[11] G. Spykman, Dry storage of spent nuclear fuel and high active waste in germany—current situation and technical aspects on inventories integrity for a prolonged storage time, Nuclear Engineering and Technology 50 (2018) 313–317. doi:https://doi.org/10.1016/j.net.2018.01.009, special issue on the water reactor fuel performance meeting 2017 (WRFPM 2017).

[12] Y. Trehub, Y. Pechera, The provision of safe storage of spent fuel from power reactors in ukraine, in: IAEA-TECDOC–1089, IAEA, International symposium on storage of spent fuel from power reactors; Vienna (Austria); 9-13 Nov 1998, 1999, pp. 29–39.

[13] Federal agency for nuclear control, Seventh meeting of the Contracting Parties to the Joint Convention on the Safety of Spent Fuel Management and on the Safety of Radioactive Waste Management, Technical Report, Kindom of Belgium, 2020.

[14] T. Ahn, V. Rondinella, T. Wiss, Potential stress on cladding imposed by the matrix swelling from alpha decay in high burnup spent nuclear fuel, Proc. IHLRWMC (2013) 111–117.

[15] T. Wiss, J.-P. Hiernaut, D. Roudil, J.-Y. Colle, E. Maugeri, Z. Talip, A. Janssen, V. Rondinella, R. J. Konings, H.-J. Matzke, W. J. Weber, Evolution of spent nuclear fuel in dry storage conditions for millennia and beyond, Journal of Nuclear Materials 451 (2014) 198–206. doi:https://doi.org/10.1016/j.jnucmat.2014.03.055.

[16] H. Assmann, R. Manzel, The matrix swelling rate of UO_2, Journal of Nuclear Materials 68 (1977) 360 – 364. doi:http://dx.doi.org/10.1016/0022-3115(77)90266-5.

[17] NEA Nuclear Science Committee Task Force, Scientific Issues of Fuel Behaviour, Fission Product Swelling, Technical Report, OECD, 1995.

[18] M. Marchetti, D. Laux, L. Fongaro, T. Wiss, P. Van Uffelen, G. Despaux, V. Rondinella, Physical and mechanical characterization of irradiated uranium dioxide with a broad burnup range and different dopants using acoustic microscopy, Journal of Nuclear Materials 494 (2017) 322–329. doi:https://doi.org/10.1016/j.jnucmat.2017.07.041.

[19] H. Kleykamp, The chemical state of LWR high-power rods under irradiation, Journal of Nuclear Materials 84 (1979) 109–117. doi:https://doi.org/10.1016/0022-3115(79)90154-5.

[20] K. Nogita, K. Une, Y. Korei, Tem analysis of pellet-cladding bonding layer in high burnup bwr fuel, Nuclear Instruments and Methods in Physics Research Section B: Beam Interactions with Materials and Atoms 116 (1996) 521–526. doi:https://doi.org/10.1016/0168-583X(96)00100-0.

[21] K. Nogita, K. Une, Formation of pellet-cladding bonding layer in high burnup bwr fuels, Journal of nuclear science and technology 34 (1997) 679–686. doi:10.1080/18811248.1997.9733726.

[22] K.-T. Kim, UO_2/Zry-4 chemical interaction layers for intact and leak PWR fuel rods, Journal of Nuclear Materials 404 (2010) 128–137. doi:https://doi.org/10.1016/j.jnucmat.2010.07.013.

[23] C. Ciszak, M. Mermoux, S. Miro, G. Gutierrez, F. Lepretre, I. Popa, K. Hanifi, I. Zacharie-Aubrun, L. Fayette, S. Chevalier, Micro-Raman analysis of the fuel-cladding interface in a high burnup PWR fuel rod, Journal of Nuclear Materials 495 (2017) 392–404. doi:https://doi.org/10.1016/j.jnucmat.2017.08.038.

[24] M. Chollet, S. Valance, S. Abolhassani, G. Stein, D. Grolimund, M. Martin, J. Bertsch, Synchrotron X-ray diffraction investigations on strains in the oxide layer of an irradiated zircaloy fuel cladding, Journal of Nuclear Materials 488 (2017) 181–190. doi:https://doi.org/10.1016/j.jnucmat.2017.03.010.

[25] C. Ciszak, L. Desgranges, P. Garcia, C. Sabathier, L. Fayette, S. Chevalier, On the origins and the evolution of the fuel-cladding bonding phenomenon in PWR fuel rods, Journal of Nuclear Materials 520 (2019) 110–120. doi:https://doi.org/10.1016/j.jnucmat.2019.04.015.

[26] W. Weber, Thermal recovery of lattice defects in alpha-irradiated UO_2 crystals, Journal of Nuclear Materials 114 (1983) 213–221. doi:https://doi.org/10.1016/0022-3115(83)90259-3.

[27] C. Poinssot, J.-M. Gras, Key scientific issues related to the sustainable management of spent nuclear fuels in the back-end of the fuel cycle, volume 1124, 2008. doi:10.1557/PROC-1124-Q02-01.

[28] M. Marchetti, Elastic properties characterization of nuclear fuels under extreme conditions, Ph.D. thesis, Montpellier, 2017.

[29] E. De Bona, A. Benedetti, O. Dieste, D. Staicu, T. Wiss, R. Konings, Radiation effects in alpha-doped UO_2, Nuclear Instruments and Methods in Physics Research Section B: Beam Interactions with Materials and Atoms 468 (2020) 54–59. doi:https://doi.org/10.1016/j.nimb.2020.01.024.

[30] M. Aomi, T. Baba, T. Miyashita, K. Kamimura, T. Yasuda, Y. Shinohara, T. Takeda, Evaluation of hydride reorientation behavior and mechanical properties for high-burnup fuel-cladding tubes in interim dry storage, Journal of ASTM International 5 (2008). doi:https://doi.org/10.1520/JAI101262.

[31] F. Rowold, K. Hummelsheim, M. Stuke, Open questions on the road to reliable predictions of cladding integrity, Kerntechnik 83 (2018) 484–487. doi:https://doi.org/10.3139/124.110952.

[32] C. Patterson, F. Garzarolli, R. Adamson, K. Coleman, Dry Storage Handbook-Fuel Performance in Dry Storage, Technical Report, Advanced Nuclear Technology International, Sweden, 2015.

[33] D. Northwood, A. Causey, Microstructural changes during thermally induced strain recovery in irradiated Zircaloy-4 stress relaxation specimens, Journal of Nuclear Materials 64 (1977) 308–312. doi:https://doi.org/10.1016/0022-3115(77)90084-8.

[34] C. Gibert, Influence de l'irradiation et de la présence de lithium sur la nature cristallographique de la zircone dans le cadre de l'étude de la corrosion du Zircaloy 4 en milieu réacteur à eau pressurisée, Ph.D. thesis, École centrale Paris, Châtenay-Malabry, France, 1999.

[35] E. Vlassopoulos, A. Pautz, S. Caruso, V. Raffuzzi, P. Grünberg, J. Helfenstein, P. Schwizer, D. Papaioannou, L. Fongaro, R. Nasyrow, R. Gretter, J. Somers, V. V. Rondinella, Mechanical integrity of spent nuclear fuel: From experimental to numerical studies, TOPFUEL 2018 30 September - 04 October 2018, Prague Czech Republic, 2018.

[36] T. König, Examination of the radionuclide inventory and chemical interactions on the interface between nuclear fuel and Zircaloy-4 cladding in irradiated LWR-fuel samples., Ph.D. thesis, Karlsruhe Institute of Technology, 2022.

[37] E. González-Robles, V. Metz, D. Wegen, M. Herm, D. Papaioannou, E. Bohnert, R. Gretter, N. Müller, R. Nasyrow, W. de Weerd, T. Wiss, B. Kienzler, Determination of fission gas release of spent nuclear fuel in puncturing test and in leaching experiments under anoxic conditions, Journal of Nuclear Materials 479 (2016) 67–75. doi:https://doi.org/10.1016/j.jnucmat.2016.06.035.

[38] D. H. Wegen, D. Papaioannou, R. Nasyrow, R. Gretter, W. De Weerd, Non-destructive testing of segment N0204 of the spent fuel pin SBS1108, Technical Report JRC75272, European Commission, Joint Research Centre, 2012.

[39] P. Rudling, A. Strasser, F. Garzarolli, L. van Swam, Welding of Zirconium alloys, ZIRAT12, Technical Report, A.N.T international, 2007.

[40] M. Herm, E. González-Robles, M. Böttle, N. Müller, D. Papaioannou, D. H. Wegen, R. Dagan, B. Kienzler, V. Metz, Description of Zircaloy-4 dissolution experiment in a shielded box, CAST CArbon-14 Source Term), Technical Report D 3.8, Karlsruhe Institute of Technology & European Commission, Joint Research Centre, Institute for Transuranium Elements, 2015.

[41] T. yang Noh, B.-G. Park, M.-S. Kim, Estimation of nuclear heating by delayed gamma rays from radioactive structural materials of HANARO, Nuclear Engineering and Technology 50 (2018) 446–452. doi:https://doi.org/10.1016/j.net.2018.01.010.

[42] F. Weise, Keramografische und Metallografische Untersuchungen des Brennstabsegments KWG-1108-N0202-RS2, Technical Report, Kernforchungszentrum Karlsruhe, HauptabteilungVersuchstechnik - HeißeZellen. Primärbericht, 1992.

[43] J. Schindelin, I. Arganda-Carreras, E. Frise, V. Kaynig, M. Longair, T. Pietzsch, S. Preibisch, C. Rueden, S. Saalfeld, B. Schmid, et al., Fiji: an open-source platform for biological-image analysis, Nature methods 9 (2012) 676–682.

[44] Y. Chang, H. Wang, Q. Zhu, P. Luo, S. Dong, Theoretical calculation and analysis of ZrO_2 spherical nanometer powders, Journal of Advanced Ceramics 2 (2013) 21–25. doi:10.1007/s40145-013-0036-2.

[45] M. Marchetti, D. Laux, A. Seibert, P. Bottomley, T. Wiss, V. Rondinella, G. Despaux, Elastic properties of severely degraded fuels, Journal of Nuclear Materials 529 (2020) 151918. doi:https://doi.org/10.1016/j.jnucmat.2019.151918.

[46] A. Ferrari, P. R. Sala, A. Fasso, R. Johannes, FLUKA: a multi-particle transport code, Technical Report, CERN-2005-10, INFN/TC_05/11, SLAC-R-773, 2005.

[47] T. T. Böhlen, F. Cerutti, M. P. W. Chin, A. Fassò, A. Ferrari, P. G. Ortega, A. Mairani, P. R. Sala, G. Smirnov, V. Vlachoudis, The FLUKA code: developments and challenges for high energy and medical applications, Nuclear data sheets 120 (2014) 211–214.

[48] V. Vlachoudis, FLAIR: a powerful but user friendly graphical interface for FLUKA, in: Proc. Int. Conf. on Advances in Mathematics, Computational Methods & Reactor Physics (M&C 2009), volume 176, Saratoga Springs, New York (United States); 3-7 May, 2009.

[49] FLUKA manual on-line, `http://www.fluka.org/content/manuals/online/INDEX-manual.html`, 2021. Accessed: 2021-09-28.

[50] L. E. Murr, Handbook of Materials Structures, Properties, Processing and Performance, Springer International Publishing, Cham, 2015, pp. 11–26. doi:10.1007/978-3-319-01815-7_2.

[51] R. D. Evans, The atomic nucleus, volume 582, McGraw-Hill New York, 1955.
[52] E. El Allam, C. Inguimbert, A. Meulenberg, A. Jorio, I. Zorkani, Gamma non-ionizing energy loss: Comparison with the damage factor in silicon devices, Journal of Applied Physics 123 (2018) 095703. doi:https://doi.org/10.1063/1.5013211.
[53] M. Guthoff, W. de Boer, S. Müller, Simulation of beam induced lattice defects of diamond detectors using fluka, Nuclear Instruments and Methods in Physics Research Section A: Accelerators, Spectrometers, Detectors and Associated Equipment 735 (2014) 223–228. doi:https://doi.org/10.1016/j.nima.2013.08.083.
[54] A. Fasso, A. Ferrari, G. Smirnov, F. Sommerer, V. Vlachoudis, Fluka realistic modeling of radiation induced damage, Progress in Nuclear Science and Technology 2 (2011) 769–775.
[55] M. Norgett, M. Robinson, I. Torrens, A proposed method of calculating displacement dose rates, Nuclear Engineering and Design 33 (1975) 50–54. doi:https://doi.org/10.1016/0029-5493(75)90035-7.
[56] K. Nordlund, A. E. Sand, F. Granberg, S. J. Zinkle, R. Stoller, R. S. Averback, T. Suzudo, L. Malerba, F. Banhart, W. J. Weber, et al., Primary Radiation Damage in Materials, Technical Report, OECD-NEA, 2015.
[57] K. Nordlund, S. J. Zinkle, A. E. Sand, F. Granberg, R. S. Averback, R. Stoller, T. Suzudo, L. Malerba, F. Banhart, W. J. Weber, et al., Improving atomic displacement and replacement calculations with physically realistic damage models, Nature communications 9 (2018) 1–8. doi:https://doi.org/10.1038/s41467-018-03415-5.
[58] K. Nordlund, A. E. Sand, F. Granberg, S. J. Zinkle, R. Stoller, R. S. Averback, T. Suzudo, L. Malerba, F. Banhart, W. J. Weber, et al. (2015).
[59] A. Konobeyev, U. Fischer, Y. Korovin, S. Simakov, Evaluation of effective threshold displacement energies and other data required for the calculation of advanced atomic displacement cross-sections, Nuclear Energy and Technology 3 (2017) 169–175. doi:https://doi.org/10.1016/j.nucet.2017.08.007.
[60] J.-P. Crocombette, D. Ghaleb, Molecular dynamics modeling of irradiation damage in pure and uranium-doped zircon, Journal of Nuclear Materials 295 (2001) 167–178. doi:https://doi.org/10.1016/S0022-3115(01)00557-8.
[61] V. V. Rondinella, T. Wiss, The high burn-up structure in nuclear fuel, Materials Today 13 (2010) 24 – 32. doi:http://dx.doi.org/10.1016/S1369-7021(10)70221-2.
[62] T. Wiss, V. V. Rondinella, R. J. M. Konings, D. Staicu, D. Papaioannou, S. Bremier, P. Pöml, O. Benes, J.-Y. Colle, P. V. Uffelen, A. Schubert, F. Cappia, M. Marchetti, D. Pizzocri, F. Jatuff, W. Goll, T. Sonoda, A. Sasahara, S. Kitajima, M. Kinoshita, Properties of the high burnup structure in nuclear light water reactor fuel, Radiochimica Acta 105 (2017) 893–906. doi:doi:10.1515/ract-2017-2831.
[63] D. H. Wegen, S. Bremier, D. Pellottiero, SEM Study on High Burn-up Fuel, Technical Report JRC104732, European Commission, Joint Research Centre, 2016.
[64] M. Marchetti, D. Laux, F. Cappia, M. Laurie, P. Van Uffelen, V. V. Rondinella, T. Wiss, G. Despaux, High frequency acoustic microscopy for the determination of porosity and Young's modulus in high burnup uranium dioxide nuclear fuel, IEEE Transactions on Nuclear Science 63 (2016) 1520–1525. doi:10.1109/TNS.2016.2552241.
[65] B. Grambow, A. Loida, P. Dressier, H. Geckeis, J. Gago, J. Casas, J. De Pablo, J. Giménez, M. Torrero, Chemical reaction of fabricated and high burn-up spent $U0_2$ fuel with saline brines, Technical Report EUR 17111 EN, European Commission, Directorate-General Science, Research and Development, 1997.
[66] U. Fischer, H. W. Wiese, Verbesserte konsistente Berechnung des nuclearen Inventars abgebrannter DWR-Brenstoffe auf der Basis vor Zell-Abbrand-Verfahren mit KORIGEN, Technical Report KfK-3014, Kernforschungszentrum Karlsruhe, 1983.
[67] U. Fischer, H. W. Wiese, Improved and consistent determination of the nuclear inventory of spent PWR fuel on the base of cell-burnup methods using KORIGEN, Technical Report TR-5043, KfK-3014, 1983.
[68] J. Magill, J. Galy, R. Dreher, D. Hamilton, M. Tufan, C. Normand, A. Schwenk-Ferrero, H. W. Wiese, Nucleonica nuclear science portal, 2007, pp. 89–92. doi:10.1051/ndata:07150.